A Simple Position-Sensorless Algorithm for Rotor-Side Field-Oriented Control of Wound-Rotor Induction Machine

Rajib Datta and V. T. Ranganathan, *Senior Member, IEEE*

***Abstract*—A simple position-sensorless method for rotor-side field-oriented control of a wound-rotor induction machine is described in this paper. The algorithm is based on axis transformations. Compared to the previously proposed methods, it is more direct and the dependence on machine parameters is also largely reduced. The algorithm can be started on the fly without the knowledge of the initial rotor position. Operation at synchronous speed, corresponding to zero rotor frequency, is stable, thus making it suitable for variable speed constant frequency operations. Simulation and experimental results show excellent performance of the scheme.**

***Index Terms*—Position-sensorless control, rotor-side control, variable-speed constant-frequency operation, wound-rotor induction machine.**

NOMENCLATURE

u_{s1}, u_{s2}, u_{s3}	Three-phase stator voltages.
u_{r1}, u_{r2}, u_{r3}	Three-phase rotor voltages.
$u_{\rm dc}$	DC-link voltage.
$\underline{u_s}$	Stator voltage vector in stator coordinate system.
$\underline{u_r}$	Rotor voltage vector in rotor coordinate system.
u_{rd}, u_{rq}	Components of $\underline{u_r}$ in stator flux coordinate system.
i_{s1}, i_{s2}, i_{s3}	Three-phase stator currents.
i_{r1}, i_{r2}, i_{r3}	Three-phase rotor currents.
$i_{s\alpha}$, $i_{s\beta}$	Components of stator current in stator coordinate system.
$i_{r\alpha}$, $i_{r\beta}$	Components of rotor current in stator coordinate system.
i_{ra}, i_{rb}	Components of rotor current in rotor coordinate system.
i_{rd}, i_{rq}	Components of rotor current in stator flux coordinate system.
$\underline{i_s}$	$= i_{s\alpha} + ji_{s\beta}$ Stator current vector in stator coordinate system.
$\underline{i_r}$	$= i_{ra} + ji_{rb}$ Rotor current vector in rotor coordinate system.
${}^s\underline{i_r}$	$= i_{r\alpha} + ji_{r\beta}$ Rotor current vector in stator coordinate system.
$\lvert{}^s\underline{i_r}\rvert$	$= \lvert\underline{i_r}\rvert$ Magnitude of rotor current vector.
$\underline{i_{ms}}$	Stator flux magnetizing current vector in stator coordinate system.
$i_{ms\alpha}$, $i_{ms\beta}$	Components of $\underline{i_{ms}}$ in stator coordinate system.
i_{ms}	Magnitude of $\underline{i_{ms}}$.
L_0, L_s, L_r	Magnetizing, stator, and rotor inductances.
R_s, R_r	Stator and rotor resistances.
T_s, T_r	Stator and rotor time constants.
σ_s, σ_r, σ	Stator, rotor, and total leakage factors.
ω_s	Grid angular frequency (electrical rad/s).
ω_m, ω	Actual speed of the rotor in mechanical, electrical rad/s.
$\omega_{\rm est}$	Estimated value of rotor speed (electrical rad/s).
ω_{ms}	Angular velocity of stator flux vector (electrical rad/s).
ρ_1	Angle of rotor current vector with respect to stator "α" axis.
ρ_2	Angle of rotor current vector with respect to rotor "a" axis.
$\in$	$= \rho_1 - \rho_2$ Rotor position (angle of rotor "a" axis with respect to stator "α" axis).
θ	Angle of stator voltage vector with respect to stator "α" axis.
μ	Angle of $\underline{i_{ms}}$ with respect to stator "α" axis (approximated as $\theta - 90$ by neglecting stator resistance drop).
K_{pr}, K_{ir}	Gains of proportional and integral terms in the current PI controllers.
P	Number of poles.
FF	Decoupling/feedforward signals in the current loops.
*	Superscript denoting reference values of corresponding variables.

Manuscript received August 8, 2000; revised February 1, 2001. Abstract published on the Internet June 6, 2001.

R. Datta was with the Department of Electrical Engineering, Indian Institute of Science, Bangalore 560 012, India. He is now with Electrical Drive Systems (DECRC/E4), ABB Corporate Research, ABB Forschungszentrum, D-69003 Heidelberg, Germany.

V. T. Ranganathan is with the Department of Electrical Engineering, Indian Institute of Science, Bangalore 560 012, India (e-mail: vtran@ee.iisc.ernet.in).

Publisher Item Identifier S 0278-0046(01)06280-3.

I. INTRODUCTION

ROTOR-SIDE control of a grid-connected wound-rotor induction machine is very attractive for variable-speed constant-frequency (VSCF) applications with limited speed range. In the system under consideration, the stator is directly

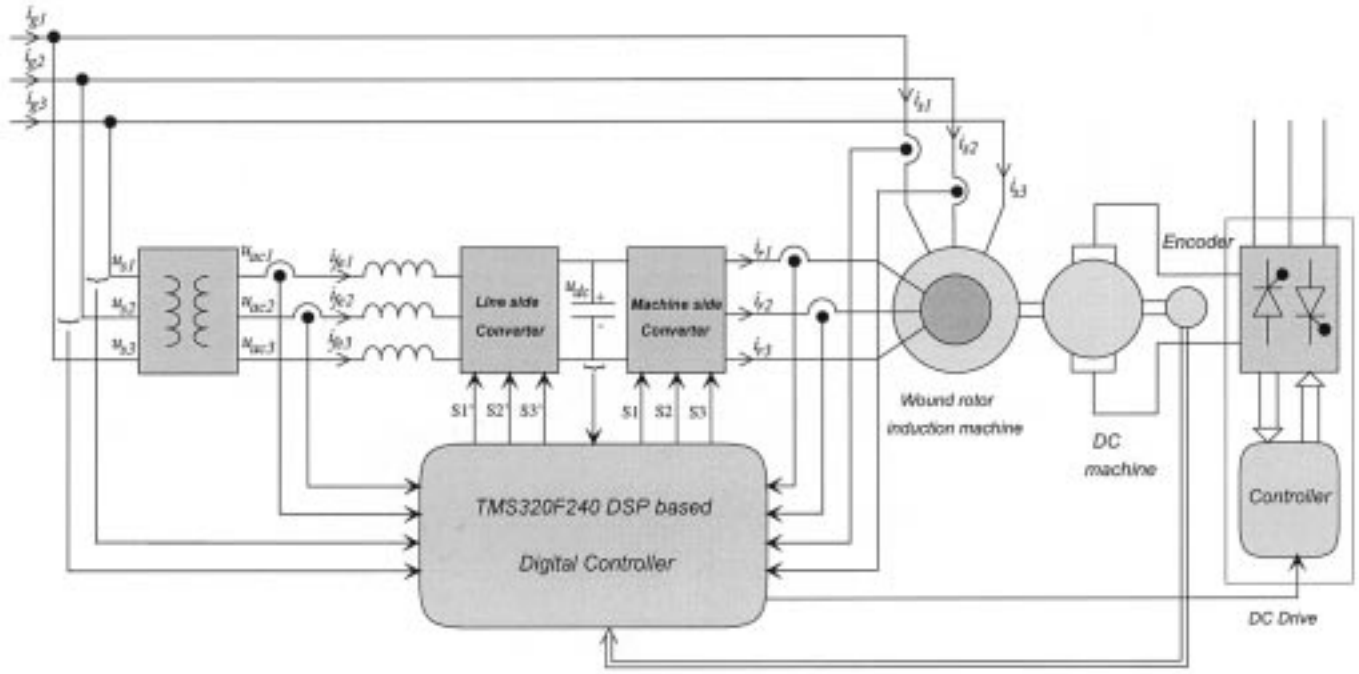

Fig. 1. Schematic block diagram of the experimental setup.

connected to the three-phase grid and the rotor is supplied by two back-to-back pulsewidth modulation (PWM) converters (Fig. 1). Such an arrangement provides flexibility of operation in subsynchronous and supersynchronous speeds both in the generating and motoring modes. The rating of the power converters used in the rotor circuit is substantially lower than the machine rating and is decided by the range of operating speed.

The requirement for VSCF operation has led to the use of rotor-side field-oriented control of wound-rotor induction machines to independently control the active and reactive powers. The conventional approach for this is stator-flux-oriented control using rotor position sensors [1], [2]. The performance of the system thus depends on the accuracy of computation of the stator flux and the accuracy of the rotor position information derived from the position encoder. Alignment of the position sensor is moreover, difficult in a doubly fed wound-rotor machine. In applications such as wind-power generation, there is a large physical separation between the generator (which is coupled to the turbine shaft through gears) and the power electronic equipment (which is at ground level). It is, therefore, desirable that there is minimum interface between the two and, for higher reliability, a control scheme without shaft position sensors.

There are two major challenges in designing a position sensorless scheme for a doubly fed wound-rotor induction machine. The foremost requirement is that the algorithm should work stably at or near synchronous speed, corresponding to very low or zero rotor frequency. The second criterion is that the algorithm should be able to start on the fly. It is understood that the rotor side control strategy operates over a restricted speed range. Therefore, with the stator connected to the grid, the control can be initiated only when the speed rises above a minimum threshold. Hence, the position estimation algorithm should start while the rotor is already in motion, without the knowledge of any initial condition.

Position sensorless vector control methods have been proposed by several research groups in the recent past [3]–[6]. The method proposed in [3] uses the rotor voltages and currents to design a torque angle controller. The major difficulty of this scheme is the method employed for computation of rotor flux. The integration of rotor voltage at or near synchronous speed, is analogous to the integration of the stator voltage at or near zero speed in the case of a cage rotor induction machine. Hence, similar problems of integrator saturation resulting in incorrect estimation of the rotor flux is inevitable. Use of this algorithm has to be restricted up to a certain minimum slip and operation through synchronous speed is not possible. The scheme proposed in [4] is by far the most comprehensive one available in the literature. The system developed (ROTODRIVE) is a commercial product aimed at the variable-speed high-power drive market ($>$300 kW). This algorithm, based on coordinate transformation, provides stable operation at or near synchronous speed and, can be started on the fly. However, the accuracy of the estimation process depends on machine parameters like L_s, R_s and the supply frequency.

In this paper, a sensorless control algorithm is proposed which is also based on axis transformations. Compared to the other methods, it is more direct and the dependence on machine parameters is also largely reduced. The algorithm can be started on the fly without the knowledge of the initial rotor position. Operation at synchronous speed, corresponding to zero rotor frequency, is stable, thus making it suitable for VSCF operations.

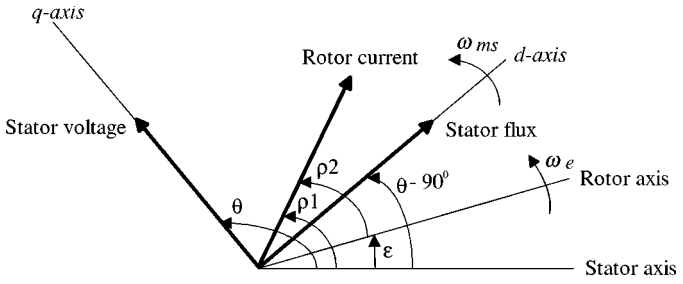

Fig. 2. Location of different vectors in stationary coordinates.

II. Control Algorithm

The proposed sensorless algorithm is explained with the help of Fig. 2. Here, the rotor current vector is shown along with the stator and rotor axes. Seen from the stator coordinate system, $\underline{i_r}$ makes an angle ρ_1. The same vector makes an angle ρ_2 with the rotor axis. The problem, therefore, is to compute ρ_1 and ρ_2, so that $\varepsilon = (\rho_1 - \rho_2)$ can be determined. With the knowledge of the stator flux and the stator currents, the rotor current in the stator reference frame, i.e., $\underline{^s i_r}$ can be computed. In the rotor reference frame $\underline{i_r}$ can be directly measured. From this information, the angle between the two reference frames can be computed by using simple trigonometric relations.

In terms of the stator and rotor currents, the stator flux magnetizing current $\underline{i_{ms}}$ [1] can be expressed as

$$\underline{i_{ms}} = (1+\sigma_s)\underline{i_s} + \underline{^s i_r}. \tag{1}$$

In Fig. 2, the stator voltage vector $\underline{u_s}$ is also shown. Assuming that the stator resistance drop is negligible, the stator flux axis, i.e., the *d axis* is at quadrature to it. Hence, the stator flux magnetizing current vector $\underline{i_{ms}}$ makes an angle $(\theta - 90^\circ)$ with the stator axis. It is assumed for the present that the magnitude of $\underline{i_{ms}}$ vector (denoted as i_{ms}) is known. (The estimation of i_{ms} is presented later.) Therefore, the α, β components can be written as follows:

$$i_{ms\alpha} = i_{ms} \cdot \sin\theta \tag{2}$$

$$i_{ms\beta} = -i_{ms} \cdot \cos\theta. \tag{3}$$

Using this value of $\underline{i_{ms}}$ and the measured value of $\underline{i_s}$, the rotor currents can be computed in the stationary coordinates as

$$i_{r\alpha} = i_{ms\alpha} - (1+\sigma_s) i_{s\alpha} \tag{4}$$

$$i_{r\beta} = i_{ms\beta} - (1+\sigma_s) i_{s\beta} \tag{5}$$

$$|\underline{^s i_r}| = \left(i_{r\alpha}^2 + i_{r\beta}^2\right)^{1/2}. \tag{6}$$

The unit vectors for $\underline{^s i_r}$ are given by

$$\cos\rho_1 = i_{r\alpha}/|\underline{^s i_r}| \tag{7}$$

$$\sin\rho_1 = i_{r\beta}/|\underline{^s i_r}|. \tag{8}$$

The rotor currents are directly measured in the rotor circuit, and the unit vectors for $\underline{i_r}$ can be derived as

$$\cos\rho_2 = i_{ra}/|\underline{i_r}| \tag{9}$$

$$\sin\rho_2 = i_{rb}/|\underline{i_r}|. \tag{10}$$

Equations (7) –(10) represent the unit vectors in the two reference frames, the former rotating at synchronous speed and, the latter at slip frequency. The unit vectors pertaining to the rotor position $\varepsilon = (\rho_1 - \rho_2)$ can now be easily computed

$$\begin{aligned}\sin\varepsilon &= \sin(\rho_1 - \rho_2) \\ &= \sin\rho_1 \cdot \cos\rho_2 - \sin\rho_2 \cdot \cos\rho_1 \end{aligned} \tag{11}$$

$$\begin{aligned}\cos\varepsilon &= \cos(\rho_1 - \rho_2) \\ &= \cos\rho_1 \cdot \cos\rho_2 + \sin\rho_1 \cdot \sin\rho_2. \end{aligned} \tag{12}$$

It may be noted here that the unit vectors $\sin\varepsilon$ and $\cos\varepsilon$ corresponding to the rotor position suffice for executing the vector control algorithm. The actual angle need not be computed through inverse functions, as in [4].

The vector control block diagram with current control is shown in Fig. 3. The rotor currents are first transformed to the stator coordinates ($e^{j\in}$) and subsequently to the field coordinates ($e^{-j\mu}$) to obtain i_{rd} and i_{rq}. The current controllers are PI controllers, followed by the addition of decoupling/feedforward signals (denoted as *FF* in Fig. 3). The full form of the controller equations are given in Appendix II. In the implementation, the grid frequency ω_s is used instead of ω_{ms} and ω_{est} instead of ω. The reference voltages u_{rd}^* and u_{rq}^* generated by the current control loops are transformed back to the rotor reference frame ($e^{j(\mu-\in)}$) and modulated with a carrier triangle to generate the PWM patterns for the rotor-side inverter.

A. Computation of i_{ms}

The accuracy of computation of $\sin^{\in}$ and $\cos^{\in}$ depends on the value of i_{ms}, since the other quantities are directly measured. The stator flux can be calculated directly by stator voltage integration so that the variations in the grid voltage and frequency are taken into account. However, in order to estimate i_{ms}, the magnetizing inductance L_o is required. If there is a substantial boost in the grid voltage, or a dip in the grid frequency, L_o is most likely to saturate. This will lead to an incorrect estimation of i_{ms}. Also, the presence of distortion components in the grid voltage normally gives rise to integration problems. The objective is, therefore, to make the estimation process minimally dependent on any machine parameter and, if possible, avoid integration of the stator voltage.

Any change in the magnitude of the stator flux being much slower than the sampling frequency (which in this case is 2.9 kHz), i_{ms} can be correctly estimated by adopting the following method of recomputation. First, i_{ms} for the present sampling interval is computed by transforming the present rotor current sample to the stator coordinates using the unit vectors computed in the previous interval. This is formulated as follows:

$$i'_{r\alpha}[k] = i_{ra}[k] \cdot \cos\varepsilon[k-1] - i_{rb}[k] \cdot \sin\varepsilon[k-1] \tag{13}$$

$$i'_{r\beta}[k] = i_{rb}[k] \cdot \cos\varepsilon[k-1] + i_{ra}[k] \cdot \sin\varepsilon[k-1] \tag{14}$$

$$i'_{ms\alpha}[k] = (1+\sigma_s) \cdot i_{s\alpha}[k] + i'_{r\alpha}[k] \tag{15}$$

$$i'_{ms\beta}[k] = (1+\sigma_s) \cdot i_{s\beta}[k] + i'_{r\beta}[k] \tag{16}$$

$$i'_{ms} = \left(i'^2_{ms\alpha} + i'^2_{ms\beta}\right)^{1/2}. \tag{17}$$

The superscript $'$ indicates intermediate variables used in the computation. i'_{ms} as calculated from (17) is passed through a

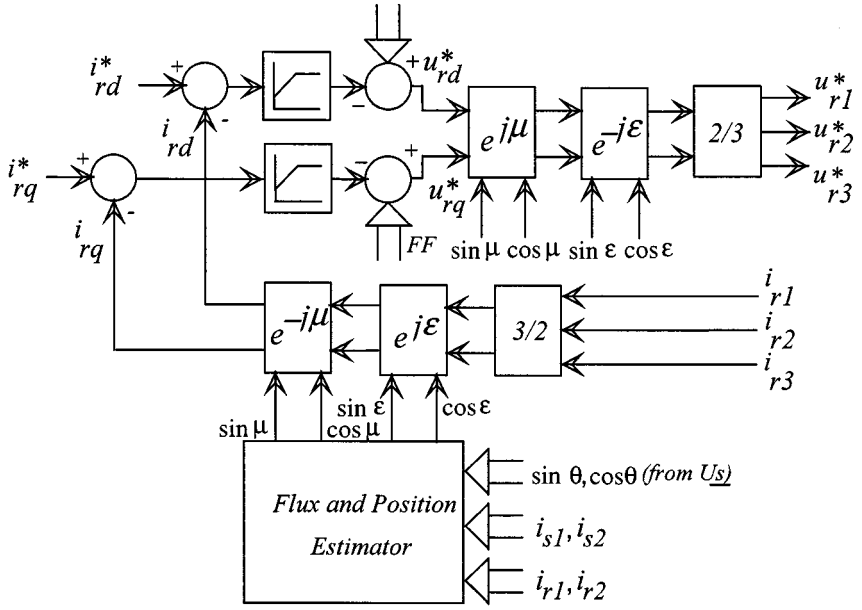

Fig. 3. Block diagram of rotor-side field-oriented control.

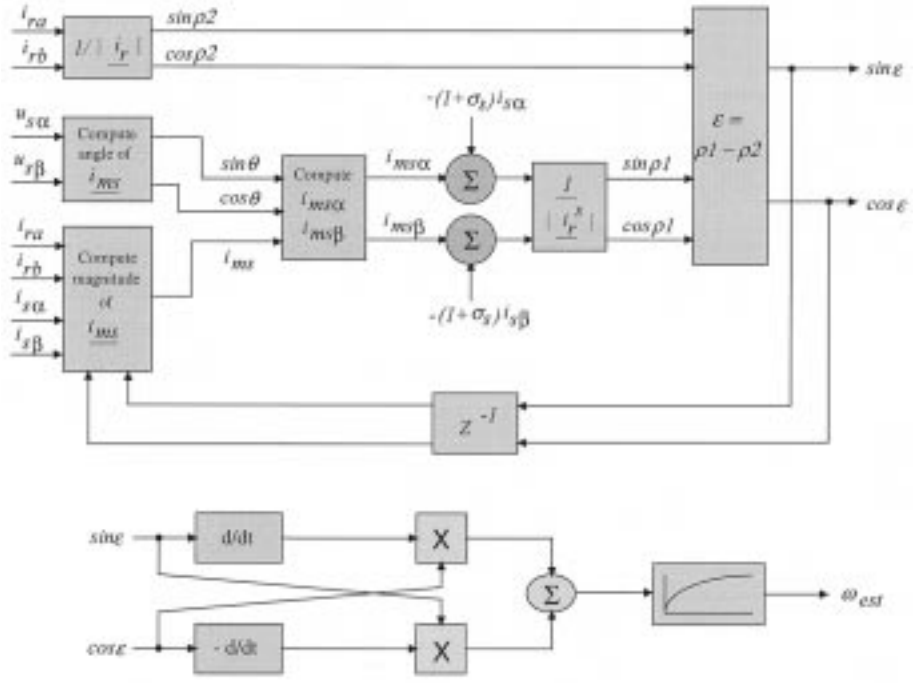

Fig. 4. Schematic block diagram of the position-sensorless algorithm.

low-pass first-order filter with a time constant of 1 ms. This ensures that even if there is any small error in the previous sample of $\sin\varepsilon$ and $\cos\varepsilon$, it is not directly reflected in the present i_{ms} estimate. The estimation of i_{ms} is the first step in the position estimation algorithm. With this value of i_{ms}, the algorithm proceeds from (1)–(11).

B. Starting

It is understood that the algorithm has to start with a known value of ε in order to compute i_{ms} by using (13)–(17). Since the rotor-side control needs to be started on the fly, it is not possible to assign an initial value of ε. Instead, the algorithm is started with an initial value of i_{ms}, which is the same as its nominal value given by $u_s/(\omega_s L_o)$. The position of i_{ms} is computed from the stator voltage phasor as before. After a few sampling intervals, the algorithm switches over to the recomputation method.

The estimation process thus becomes independent of variations in the stator voltage and frequency. The only machine parameter on which the algorithm depends is the stator leakage factor σ_s. The leakage is only a small percentage of the stator inductance and is not subjected to any saturation. Even a significant error in the value of σ_s does not introduce any appreciable error in the estimation of $\sin\varepsilon$ and $\cos\varepsilon$. This is verified through

simulation as discussed later. The instantaneous nature of computation also ensures jitter-free estimation during transients in the active and reactive power.

C. Speed Estimation

With the decoupling terms associated with the rotor current controller being slip dependent, it is necessary to compute the speed of the machine. Apart from regular motor drive applications, the speed information is also necessary for generation applications like wind-energy conversion systems where the active power reference is made to vary as a function of the rotor speed to achieve maximum power transfer. The speed can be estimated by using the following equation:

$$\omega_{est} = \cos\varepsilon \cdot \frac{d}{dt}\sin\varepsilon - \sin\varepsilon \cdot \frac{d}{dt}\cos\varepsilon. \tag{18}$$

The usual method of differentiation of rotor position would require ε to be computed from the unit vectors using inverse trigonometric functions. This is avoided in this method of speed estimation. Moreover, the unit vectors are smoothly varying continuous functions unlike ε (which is discontinuous at $\varepsilon = 2\pi$) and are easier to differentiate without checking for discontinuity. However, the differential terms contribute to some noise which is eliminated by employing a first-order low-pass filter. The position and speed estimation block diagrams are shown in Fig. 4.

The simulation of the system has been carried out on a MATLAB-SIMULINK platform to study the starting and the effect of parameter variation on the proposed algorithm. The machine and controller parameters selected are the same as used in the laboratory experimental setup (see Appendix III). Generating mode of operation is considered in the present case.

Fig. 5(a) and (b) shows the effect of variation in σ_s on the estimation process. In the first case, σ_s used in the estimation algorithm is 1.5 times the actual value and, in the second case, it is 0.5 times. The plots show almost negligible errors in the computation of the unit vectors, even at starting.

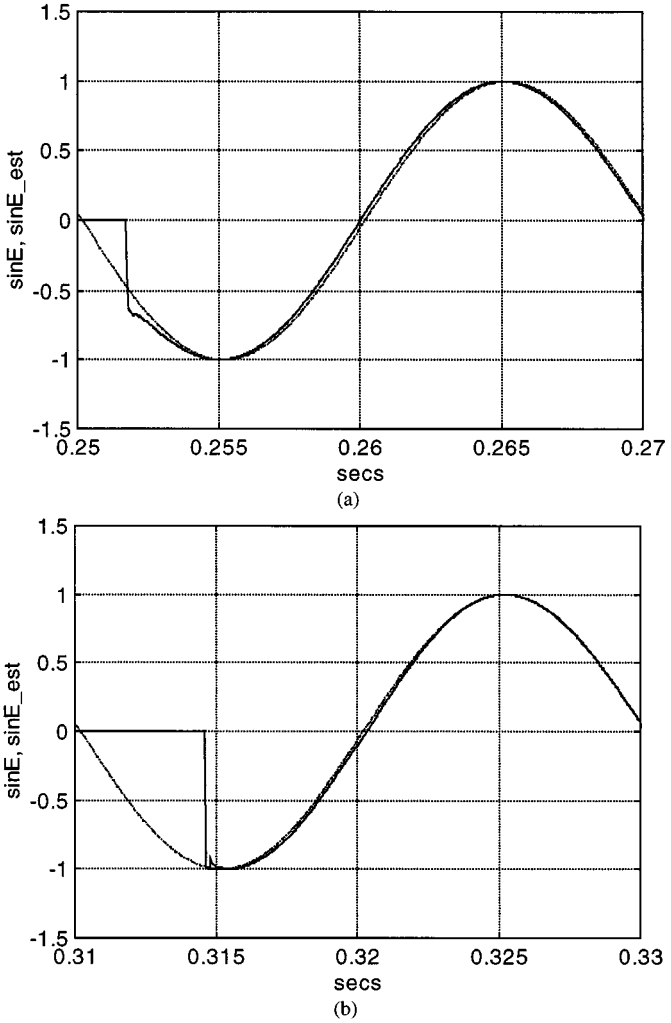

Fig. 5. Simulated waveforms of estimated (solid lines) and actual (dotted lines) $\sin\varepsilon$ when (a) value of σ_s used in computation equals 1.5 times the actual and (b) value of σ_s used in computation equals 0.5 times the actual value.

III. Experimental Implementation and Results

The schematic block diagram of the laboratory experimental setup is already shown in Fig. 1. It consists of a 3.5-kW wound-rotor induction machine with its stator connected to the 415-V 50-Hz $3-\phi$ power grid, and the rotor being fed by two back-to-back insulated-gate-bipolar-transistor (IGBT)-based PWM converters. The setup is organized for generation operation where the torque–speed characteristics of the prime mover (such as a wind turbine) is simulated by a 5-hp dc motor driven by a commercial four-quadrant thyristor drive. A *TMS320F240* digitall-signal-processor (DSP)-based digital control platform is designed and employed for implementing the position sensorless algorithm. The front-end converter control and simulation of the turbine characteristics are also executed by the same processor. Since there are several control loops involved, the software is organized for multitasking. The processor runs at a clock frequency of 36 MHz and the sampling frequency for the position control algorithm is 336 μs. The software is assembly coded for fast real-time execution.

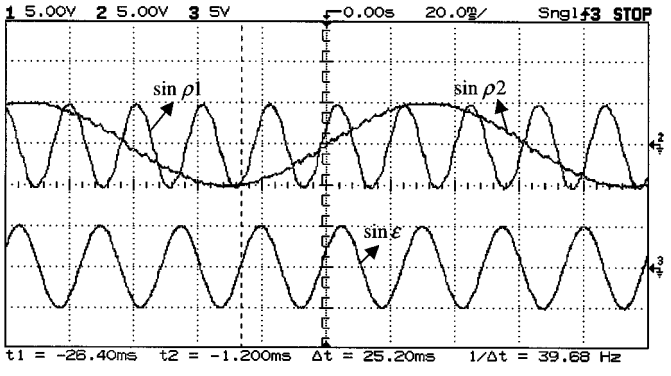

Fig. 6. Experimental waveforms showing $\sin\rho_1$, $\sin\rho_2$, and $\sin\varepsilon$ for $\omega = 1190$ rpm.

The steady-state relations between $\sin\rho_1$, $\sin\rho_2$, and $\sin\varepsilon$ are given in Fig. 6. It is observed from these plots that the frequency of $\sin\varepsilon$ is the difference of the frequencies of $\sin\rho_1$ and $\sin\rho_2$.

A comparison between the unit vector $\sin\varepsilon$ generated using an incremental position encoder with $\sin\varepsilon$ computed employing the proposed sensorless algorithm is given in Fig. 7. The plots

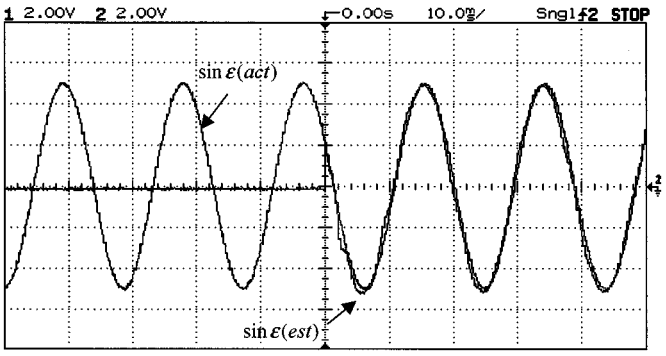

(a)

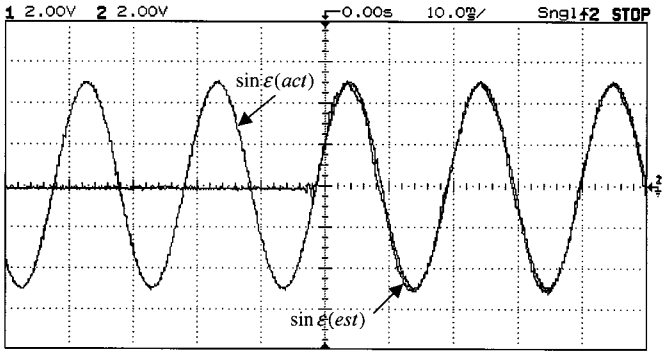

(b)

Fig. 7. Experimental waveforms showing estimated and actual $\sin\varepsilon$ at starting for (a) $\omega = 1460$ r/min and (b) $\omega = 1600$ r/min.

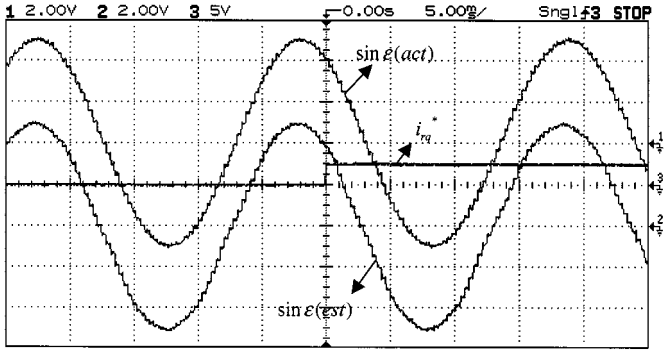

Fig. 8. Experimental waveforms showing estimated and actual $\sin\varepsilon$ for step in i_{rq}^* from 0 to 0.5 p.u.

given in Fig. 7(a) and (b) correspond to synchronous and super-synchronous modes of operation. The instantaneous tracking of the position (when the rotor side control is activated) and accurate steady-state operation are observed.

In Fig. 8, the impact of sudden active load on the estimation algorithm is shown. A step change of i_{rq}^* from 0 to 0.5 p.u. does not produce any transient in the estimation of $\sin\varepsilon$.

The estimated speed signals (from $\sin\varepsilon$ and $\cos\varepsilon$) before and after filtering are shown in Fig. 9(a) and (b). During the initial period, there is a large error in the estimated speed due to the filter time constant. If this incorrect value of estimated speed is used to determine the slip-dependent cross-coupling terms in the rotor current control, it will give rise to undesired transients and, in turn, erroneous estimation. In practice, the estimated position would not be able to catch up with the actual position. Hence,

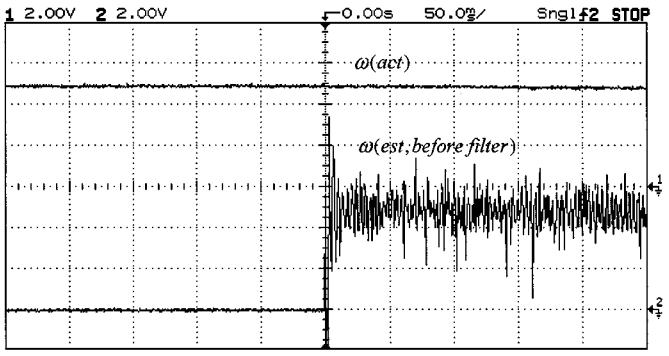

(a)

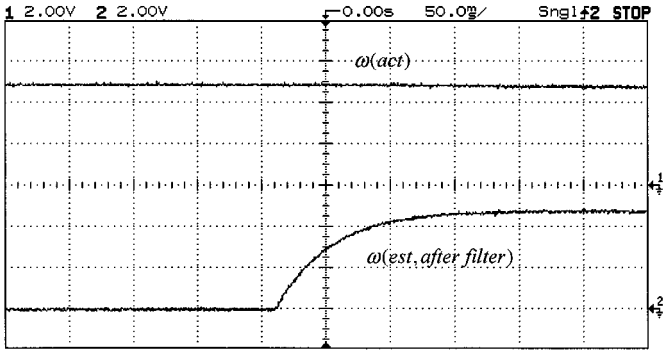

(b)

Fig. 9. Experimental waveforms showing estimated and actual ω at starting (a) before filtering and (b) after filtering.

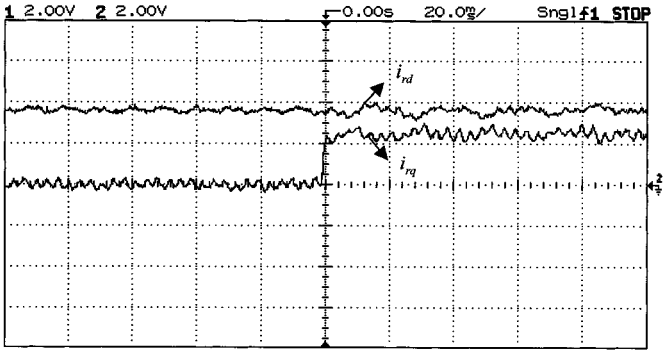

(a)

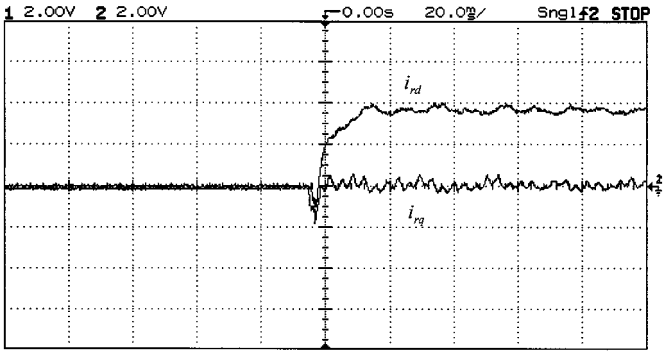

(b)

Fig. 10. Experimental results showing (a) step in i_{rq}^* from 0 to 0.5 p.u. with $i_{rd}^* = 0.75$ p.u. and (b) showing step in i_{rd}^* from 0 to 0.75 p.u. and $i_{rq}^* = 0$.

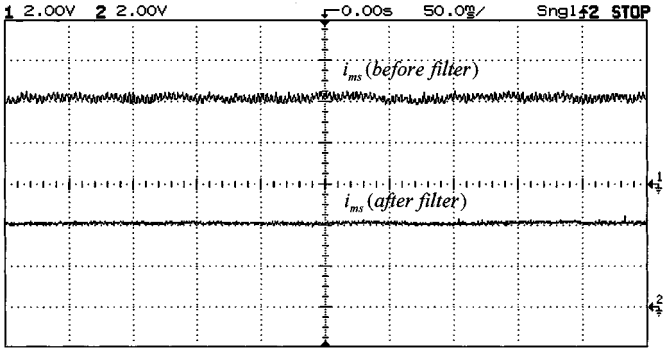

Fig. 11. Experimental results showing steady-state i_{ms} before and after filtering.

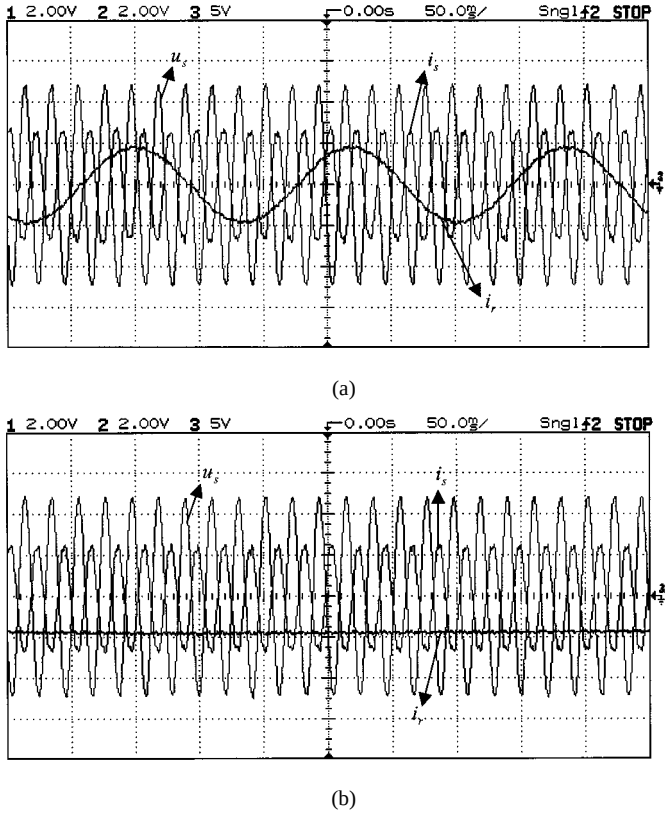

Fig. 12. Experimental results showing steady-state u_{s1}, i_{s1}, and i_{r1} with $i^*_{rd} = 0.75$ p.u. and $i^*_{rq} = 05$ p.u. at (a) 1620 r/min (supersynchronous operation) and (b) 1428 r/min (synchronous operation).

during starting the computed slip is forced to zero for about 100 ms; after this, the estimated speed signal is used to calculate the slip.

The transient response of the q-axis and d-axis rotor current loops are shown in Fig. 10(a) and (b), respectively. In Fig. 10(b), the response is taken during switching on of the rotor converter, hence, a small transient is observed in the rotor currents (before the estimated position catches up with the actual one).

Fig. 11 shows the estimated i_{ms} before and after the low-pass filter.

In Fig. 12(a) and (b), the steady-state stator and rotor currents in their own reference frames are shown along with the stator voltage waveform for supersynchronous and synchronous modes of operation. The reactive power is supplied from the rotor side, hence, the stator power factor is unity. In Fig. 12(b), the rotor currents are dc, showing that the estimation algorithm operates stably at zero rotor frequency. The transition through synchronous speed is also observed to be smooth, as is illustrated in Fig. 13.

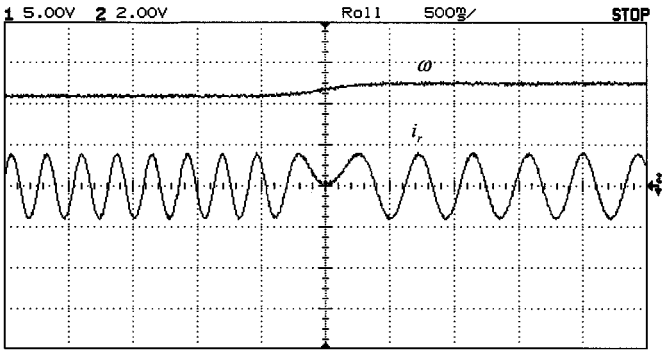

Fig. 13. Experimental results showing i_{r1}, ω during transition through synchronous speed.

IV. Conclusion

Position-sensorless control of wound-rotor induction machines is a desirable feature of VSCF generation systems like wind power generation. The proposed position-sensorless algorithm meets the requirements for such applications. The algorithm can be started on the fly without the knowledge of the initial rotor position. Operation at synchronous speed, corresponding to zero rotor frequency, is stable; also, it can ride through synchronous speed smoothly. The proposed method of computation of stator flux magnetizing current makes the estimation process independent of critical machine parameters. The simulation and experimental results show that the dynamic performance of the system compares well with that using position sensors.

Appendix I

The slip-ring induction machine equations in the stator flux (d–q) coordinates [1] are as follows:

stator:

d-axis:

$$T_s \frac{di_{ms}}{dt} + i_{ms} = \frac{1+\sigma_s}{R_s} u_{sd} + i_{rd} \tag{A1.1}$$

q-axis:

$$\frac{d\mu}{dt} = \omega_{ms} = \frac{1}{T_s i_{ms}} \left[\frac{1+\sigma_s}{R_s} u_{sq} + i_{rq} \right] \tag{A1.2}$$

rotor:

d-axis:

$$\sigma T_r \frac{di_{rd}}{dt} + i_{rd} = \frac{u_{rd}}{R_r} + (\omega_{ms} - \omega)\sigma T_r i_{rq} - (1-\sigma) T_r \frac{di_{ms}}{dt} \tag{A1.3}$$

q-axis:

$$\sigma T_r \frac{di_{rq}}{dt} + i_{rq} = \frac{u_{rq}}{R_r} - (\omega_{ms} - \omega)\sigma T_r i_{rd} - (\omega_{ms} - \omega)(1-\sigma) T_r i_{ms} \tag{A1.4}$$

mechanical:

$$J\frac{d\omega_m}{dt} = -\frac{2}{3}\frac{P}{2}\frac{L_0}{1+\sigma_s} i_{ms} i_{rq} - m_{load} \quad \text{(A1.5)}$$

$$\frac{d\in}{dt} = \omega = \frac{P}{2}\omega_m. \quad \text{(A1.6)}$$

APPENDIX II

The current-controller equations including decoupling terms are as follows:

d-axis:

$$u_{rd}^* = K_{pr}(i_{rd}^* - i_{rd}) + K_{ir}\int (i_{rd}^* - i_{rd})\,dt - (\omega_{ms} - \omega)\sigma L_r i_q \quad \text{(A2.1)}$$

q-axis:

$$u_{rq}^* = K_{pr}(i_{rq}^* - i_{rq}) + K_{ir}\int (i_{rq}^* - i_{rq})\,dt + (1-\sigma)L_r(\omega_{ms} - \omega)i_{ms} + (\omega_{ms} - \omega)\sigma L_r i_{rd}. \quad \text{(A2.2)}$$

APPENDIX III

The slip-ring induction machine data are as follows:

rated power	3 kW
stator	415 V, Δ connected, 7.2 A
rotor	415 V, Y connected, 6.6 A

$R_s = 1.557\,\Omega, \quad R_r = 2.62\,\Omega$

$L_0 = 177\,\text{mH}, \quad \sigma_s = 0.1017.$

REFERENCES

[1] W. Leonhard, *Control of Electrical Drives*. Berlin, Germany: Springer-Verlag, 1985, ch. 13.

[2] R. Pena, J. C. Clare, and G. M. Asher, "Doubly fed induction generator using back-to-back PWM converters and its application to variable-speed wind-energy generation," *Proc. Inst. Elect. Eng.*, pt. B, vol. 143, no. 3, pp. 231–241, May 1996.

[3] L. Xu and W. Cheng, "Torque and reactive power control of a doubly fed induction machine by position sensorless scheme," *IEEE Trans. Ind. Applicat.*, vol. 31, pp. 636–642, May/June 1995.

[4] L. Morel, H. Godfroid, A. Mirzaian, and J. M. Kauffmann, "Double-fed induction machine: converter optimization and field oriented control without position sensor," *Proc. Inst. Elect. Eng.*, pt. B, vol. 145, no. 4, pp. 360–368, July 1998.

[5] E. Bogalecka, "Power control of a double fed induction generator without speed or position sensor," in *Conf. Rec. EPE*, 1993, pt. 8, vol. 377, ch. 50, pp. 224–228.

[6] R. Datta, "Rotor side control of grid-connected wound rotor induction machine and its application to wind power generation," Ph.D. dissertation, Dept. Elect. Eng., Indian Inst. Science, Bangalore, India, Feb. 2000.

Rajib Datta received the B.E degree in electrical engineering from Jadavpur University, Calcutta, India, the M.Tech degree in electrical engineering from Indian Institute of Technology, Kharagpur, India, and the Ph.D. degree from Indian Institute of Science, Bangalore, India, in 1992, 1994, and 2000, respectively.

From January 1995 to July 2000, he was a Research Scholar in the Department of Electrical Engineering, Indian Institute of Science, Bangalore, India. He is currently a Research Scientist in the ABB Corporate Research Centre, Heidelberg, Germany. His research interests include power electronics, motor drives, and wind power generation.

V. T. Ranganathan (M'87–SM'92) received the B.E and M.E degrees in electrical engineering from Indian Institute of Science, Bangalore, India, and the Ph.D degree from Concordia University, Montreal, PQ, Canada.

In 1984, he joined the Electrical Engineering Department, Indian Institute of Science, Bangalore, India, where he is currently a Professor. His research interests are in the areas of power electronics and motor drives. He has authored several published papers in the areas of vector control of ac drives, PWM techniques, split-phase induction motor drives, and rotor-side control of slip-ring induction motors. He is also a Consultant to industry in the afore-mentioned areas and has participated in a number of research and development projects.

Prof. Ranganathan has received a Prize Paper Award from the Static Power Converter Committee of the IEEE Industry Applications Society and The Tata Rao Prize from the Institution of Engineers, India. He is a Fellow of The Institution of Engineers, India.